Dalton Transactions

PAPER

View Article Online
View Journal

Cite this: DOI: 10.1039/c3dt52975d

Pyridine imines as ligands in luminescent iridium complexes†

David L. Davies,*[a] Francesco Lelj,[b] Mark P. Lowe,[a] Karl S. Ryder,[a] Kuldip Singh[a] and Shalini Singh[a]

Received 22nd October 2013,
Accepted 5th January 2014

DOI: 10.1039/c3dt52975d

www.rsc.org/dalton

Biscyclometallated iridium complexes $[Ir(ppz)_2(X\hat{}Y)][PF_6]$ (X^Y = pyridine imine) have been synthesised. The pyridineimine ligands are prepared *in situ* during the complexation. The complexes show room temperature emission between 640 and 780 nm in CH_2Cl_2 solution. The emission is red shifted compared with the analogous bipyridine complex $[Ir(ppz)_2(bipy)][PF_6]$. DFT calculations have been used to shed light on the influence of the imine substituent on the electrochemical and photochemical properties. In particular, the calculations suggests that there is a significant change in geometry between the ground state and the first triplet excited state for arylimines but not for alkylimines, leading to much weaker emission for the arylimine complexes. The work demonstrates that pyridineimines can be used as a substitute for bipyridines in luminescent iridium complexes.

Introduction

Following the report by Thompson *et al*. in 1999[1] of an OLED containing cyclometalated iridium complex $[Ir(ppy)_3]$ (Hppy = 2-phenylpyridine) as a dopant there has been a huge upsurge of interest in complexes $[Ir(C\hat{}N)_3]$ and $[Ir(C\hat{}N)_2(X\hat{}Y)]$. Cationic complexes $[Ir(C\hat{}N)_2(X\hat{}Y)]^+$ have also been used in light emitting electrochemical cells.[2] The luminescence of these complexes can be tuned by altering the heterocycle, the degree of conjugation in the C^N ligand and/or the ancillary ligand and by the use of substituents on the cyclometalated phenyl, the directing heterocycle or the ancillary ligands or indeed combinations of these.[3] In cationic complexes $[Ir(C\hat{}N)_2(X\hat{}Y)]^+$ the X^Y ligand has been usually a bipyridine or phenanthroline or substituted derivative, with some examples of pyridine imidazoles,[4] pyridine pyrazoles,[5] and pyridine triazoles.[6] However, changing substituents on a bipyridine is time-consuming from a synthetic viewpoint, hence, finding an alternative to bipyridine ligands that can be easily modified may expand the usefulness of these complexes. Pyridineimines are attractive alternatives since they have similar properties to bipyridines (NN donor set and empty π*-orbitals) yet are much easier to prepare by a simple condensation between pyridine-2-carboxaldehyde and the relevant primary amine. The ready availability of different amines and the one step preparation of pyridineimines should allow much easier access to a wide variety of different substituents in comparison to bipyridines Despite these attractive properties, pyridineimines are much less explored than bipyridine complexes.

Ruthenium complexes of general type **1** and **2** have been reported.[7] Complex **1** (R = Ph) displays a reversible Ru(II)/(III) oxidation and a pyridineimine ligand centred reduction, the redox potentials being approximately 0.1 and 0.35 V more anodic than the corresponding ones in $[Ru(bipy)_3]^{2+}$.[7e] These data indicate that a pyridineimine is a better π-acceptor than bipyridine; calculations suggest that the LUMO of a pyridineimine is about 0.2 eV lower in energy than that of bipyridine.[7d] Complex **1** (R = Me) shows a similar effect but the shift to positive potentials is smaller than for R = Ph.[7c] Replacing another bipyridine with a pyridineimine, complex **2**, shifts the oxidation and reduction to even more anodic potentials.[7c,d] The π-acceptor properties of the pyridineimine are also manifest in the ^{3}MLCT emission of **1**(R = Ph) which occurs at 770 nm, a 155 nm red shift in emission compared to $[Ru(bipy)_3]^{2+}$ (λ_{em} = 615 nm) again consistent with a lower LUMO level in **1**.[7e] The synthesis of complexes **1** and **2** and their luminescence suggests that pyridineimines are useful substitutes for bipyridine in luminescent metal complexes.

[a]Department of Chemistry, University of Leicester, University Road, Leicester LE1 7RH, UK. E-mail: dld3@le.ac.uk
[b]La.M.I. and LaSCAMM, INSTM Sezione Basilicata, Dipartimento di Scienze, Università della Basilicata, Via dell'Ateneo Lucano 10, 85100 Potenza, Italy

†Electronic supplementary information (ESI) available. CCDC 922554–922560. For ESI and crystallographic data in CIF or other electronic format see DOI: 10.1039/c3dt52975d

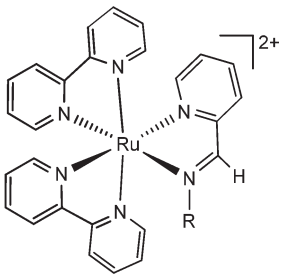

1

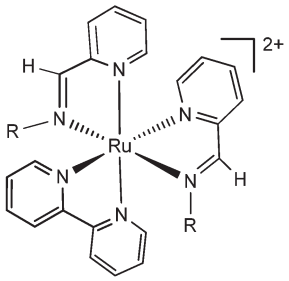

2

Recently some biscyclometallated iridium complexes with salicylimine ligands have been reported which show interesting photophysical properties, including enhanced emission in the solid state in some cases.[8] However, the first examples of pyridineimines as ligands in biscyclometallated iridium complexes was only reported last year.[9] Here we report the preparation and characterisation of some examples of complexes $[Ir(C^N)_2(X^Y)][PF_6]$(X^Y = pyridine imine) and some preliminary findings of their luminescence which show that the electrochemical and photophysical properties are affected by the substituents on the imine.

Results and discussion

Synthesis

Our first attempts at preparation involved synthesis of the pyridine imine ligand followed by complexation with the appropriate $[Ir(C^N)_2Cl]_2$ dimer. Thus, dimer **3a**, KPF_6 and the ligand (R^2 = iPr), were heated in ethanol under microwave irradiation for 30 min at 100 °C to form compound **8a** in 85% yield. Having established that the reaction worked well, the possibility of forming the ligand *in situ* was investigated. The reactions of dimers **3a–c** with pyridine-2-carboxaldehyde and the relevant amine and KPF_6 were carried out in methanol at 60 °C under microwave irradiation for 20 min, to form compounds **4a–c**, **5a–9a** in good (>80%) yields (Scheme 1). In these reactions it is not known whether the free pyridineimine ligands are generated *in situ* or they are formed after coordination of pyridine-2-carboxaldehyde to the metal.[10] The success of this *in situ* method, in principle, allows a high throughput screening approach to be used for the synthesis of analogs.[11]

The ^1H and ^{13}C NMR spectra of complexes **4–9** are very complicated due to the loss of C_2-symmetry present in the dimers, hence, in principle, all the protons of the C^N ligands and those of the pyridine are inequivalent. Nevertheless through the use of TOCSY, NOESY, COSY and HSQC we have been able to assign the vast majority of signals in each case. The features of complex **4b** (R^2 = *p*-C_6H_4Br) are explained in detail. Important parts of the NOESY spectrum are shown in Fig. 1 whilst important parts of the TOCSY, COSY and HSQC spectra are in the ESI (Fig. S1a–c†).

We have established that in complexes of type, $[Ir(C^N)_2(X^Y)]$ in addition to the characteristic high field shifts for the phenyl protons next to the metal,[12] there are NOEs that are characteristic of the $[Ir(C^N)_2]$ fragment. Hence, as expected there is an NOE between the two rings of a cyclometallating ligand *i.e.* between the phenyl proton H_d and pyrazole proton H_e (similarly $H_{d'}$ and $H_{e'}$). Phenyl protons H_a and $H_{a'}$ are observed at high field[12] (δ 6.09 and 5.93 respectively) and show weak NOEs to the pyrazole of the other cyclometallating ligand (*i.e.* to $H_{g'}$ and H_g respectively). In **4b**, $H_{a'}$ is to higher field than H_a since it is affected by the ring current of the neighbouring *N*-aryl substituent on the imine, confirmed by an NOE between $H_{a'}$ and the *ortho* protons ($H_{6/6'}$) of the (*p*-C_6H_4Br) substituent on the imine. In addition to these features, the imine proton H_5 is easily identified as the most downfield singlet, at δ 9.21. This signal also shows an NOE to the same *ortho* protons ($H_{6,6'}$). H_5 and to pyridine proton, H_4, which is observed as a doublet of doublets at δ 8.38, and a

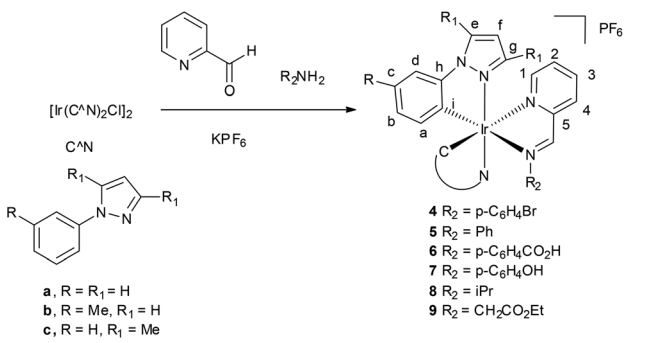

Scheme 1 Preparation of complexes **4–9** with NMR labelling scheme.

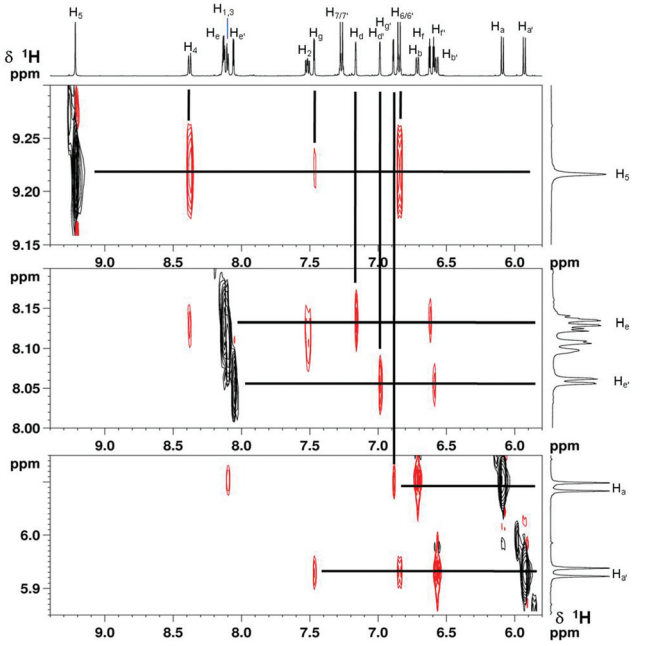

Fig. 1 Important parts of the NOESY spectrum of **4b**.

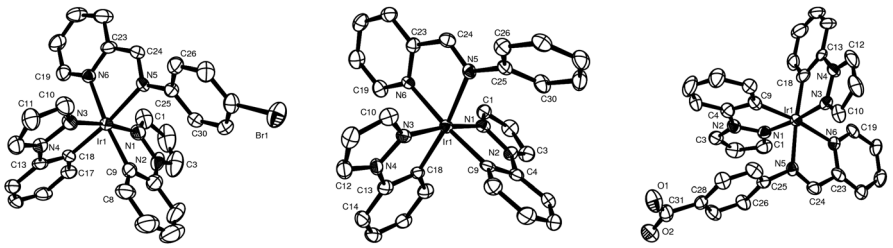

Fig. 2 X-ray structures of the cations of **4a**, **5a** and **6a** with 50% displacement ellipsoids, all H atoms omitted for clarity.

weak NOE to a doublet at δ 7.46 which is therefore assigned to the pyrazole proton which is pointing over the imine nitrogen *i.e.* H_g. $H_{g'}$ is observed at a higher field than H_g (δ 6.88 compared to δ 7.46), because it is shielded by the ring current of the pyridyl ring confirmed in the X-ray structure. Assignment of the methyl groups (Me and Me′) is possible due to the observation of an NOE between protons $H_{b,d}$ and Me and between $H_{b',d'}$ and Me′. The ^{13}C NMR spectra show the expected number of signals for the quaternary and CH carbons. The FAB mass spectrum shows a molecular ion for the cation at *m*/*z* 767.

The ^{1}H NMR spectra of **4a** and **4c** are similar to **4b**. The imine proton H_5 is the most downfield signal in each case (δ 9.33 and 9.20 respectively) and NOEs are similar to those observed in **4b**. The cyclometallated phenyl signals for **4a** and **4c** are slightly more complex than for **4b**, having an extra proton in place of the methyl, whilst for **4c** four pyrazole protons are replaced by four methyl signals, two on each pyrazole. The ^{13}C NMR spectra show the expected signals and the FAB mass spectra show peaks for the cations.

The ^{1}H and ^{13}C NMR spectra of **5a–7a** (R^2 = Ph, *p*-C_6H_4OH, *p*-$C_6H_4CO_2H$) are very similar to **4a** and also to each other except the signals of the R-groups. In all the complexes the imine proton, H_5 is always the most downfield signal (between δ 9.43 to 9.19) and the phenyl protons $H_{a,a'}$ are the most upfield (δ 6.06–6.27) and the key NOEs are similar to those in **4b** discussed above. The only significant difference in the spectra is the chemical shift of the *N*-aryl *meta* protons $H_{7/7'}$ which vary from *ca.* δ 6.5 for R = OH through to δ 7.6 (R = CO_2H), consistent with similar shifts for the free arylamines.[13] The ^{13}C NMR spectra show the expected signals and the FAB mass spectra show peaks for the cations in each one of these.

The ^{1}H NMR spectra of the alkyl substituted complexes **8a** and **9a** are similar to **4a–7a** with the phenyl protons $H_{a,a'}$ at high field (*ca.* δ 6.2–6.4). The imine proton H_5 is the most downfield signal (δ 9.28 and 9.16 respectively) and it shows an NOE to the isopropyl substituent (**8a**) or to the CH_2 (**9a**). In **8a** the two methyl groups (δ 1.12 and 1.01) are inequivalent, whilst in **9a** the diastereotopic protons of the NCH_2 group are observed as two mutually coupled doublets (δ 4.60 and 4.42), in both cases consistent with the chirality at the metal centre. The ^{13}C NMR spectra show the expected signals and the FAB mass spectrum shows a molecular ion for the cations at *m*/*z* 627 for **8a** and *m*/*z* 671 for **9a.**

X-ray crystal structures

Several of the complexes have been characterised by X-ray crystallography. The structures of **4a**, **5a**, and **6a**, are shown in Fig. 2 and those of **8a** and **9a** are shown in Fig. 3 with selected bond lengths and angles in Table 1 (those of **4b** and **4c** are in the ESI Fig. S2†). The structures show the same general features with *cis* metallated carbons and *trans* nitrogen atoms, as found for the bipyridine complexes.[2c,14] The complexes are all chiral and both enantiomers are observed in the unit cell. The iridium has a distorted octahedral geometry reflecting the fact that the three bidentate ligands have chelate angles of *ca*. 75–80°. As expected, in all cases the Ir–N bonds *trans* to C are significantly longer than those *cis* to C. The N=C imine bond length [N(5)–C(24)] is similar in all the complexes. The N(5)–C(25) bond length (from imine N to the substituent) varies between 1.426(6) Å and 1.452(10) Å,[15] in the aryl complexes whilst for the two alkyl complexes **8a** and **9a** it is 1.497(7) Å and 1.500(13) Å respectively. Hence, it is significantly shorter *ca.* 0.06 Å in the aryl complexes suggesting some delocalisation occurs in these complexes. On the other hand, in complexes **4–6** the aryl substituent is rotated out of the plane of the pyridine imine (torsion angle C(24)–N(5)–C(25)–C(26) is 44 to 60°) showing there is not complete delocalisation with the imine.

Geometries of the cations of **4a–9a** have been calculated in the low spin configuration. The computed geometries compare well with the X-ray ones. For example, in the case of **4a** (see Table S2 and Fig. S3a,b†) among the non-hydrogen atoms the largest absolute deviations of the bond distances are 0.0818 and 0.060 Å corresponding to *d*(Ir–N5) and *d*(Ir–N6) respectively, *i.e.* the Ir–N bonds to the pyridineimine ligand. Taking into account the PF_6^- counter ion the structure shows a better agreement for the Ir–N5 and Ir–N6 bonds suggesting that the pyridine imine ligand is rather sensitive to the local

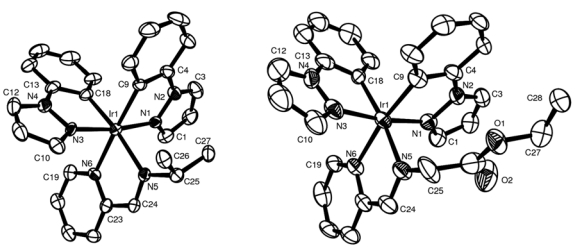

Fig. 3 X-ray structures of the cations of **8a**, and **9a** with 50% displacement ellipsoids, all H atoms omitted for clarity.

Table 1 Selected bond lengths (Å) and bond angles (°)

	4a (p-C_6H_4Br)	**5a** (C_6H_5)	**6a** (p-$C_6H_4CO_2H$)[a]	**8a** (^{i}Pr)	**9a** (CH_2CO_2Et)
Ir(1)–N(1)	2.003(4)	2.003(4)	2.035(8)	2.028(5)	2.009(8)
Ir(1)–N(3)	2.021(4)	2.020(4)	2.025(8)	2.034(4)	2.031(9)
Ir(1)–N(5) im	2.157(4)	2.143(4)	2.127(7)	2.166(4)	2.097(8)
Ir(1)–N(6) py	2.135(4)	2.124(4)	2.027(7)	2.133(4)	2.158(8)
Ir(1)–C(9)	2.027(5)	2.009(5)	1.998(10)	2.029(6)	2.022(9)
Ir(1)–C(18)	2.023(5)	2.020(5)	2.017(9)	2.010(5)	2.038(10)
N(5)–C(24)	1.288(6)	1.272(7)	1.282(11)	1.277(7)	1.297(12)
N(5)–C(25)	1.426(6)	1.436(6)	1.428(11)	1.497(7)	1.500(13)
N(1)–Ir(1)–N(3)	172.3(2)	171.4(2)	173.6(3)	171.5(2)	171.7(3)
N(1)–Ir(1)–C(9)	81.6(2)	79.7(2)	80.7(3)	79.5(2)	80.6(4)
N(3)–Ir(1)–C(18)	80.4(2)	79.7(2)	79.9(4)	80.7(2)	79.6(4)
N(5)–Ir(1)–N(6)	76.5(2)	76.5(2)	76.9(3)	75.8(2)	76.7(3)
Torsion[b]	46.7	48.9	56.7 (−59.6)		

[a] Average values from two independent molecules in the unit cell. [b] Torsion angle C(24)–N(5)–C(25)–C(26).

environment. Other distances are in fair agreement with the experimental ones being in the range 0.0 to 0.02 Å whilst the majority (72%) of the bond angles excluding hydrogen atoms are within 1.0° compared to the experimental ones (see Fig. S3a,b†). Larger differences were found in cases where the experimental values were less well defined.

The computed phenyl torsion angle (θ) of the p-Br-phenyl substituent is 43.4° which is close to the experimental value of 46.7°. Another parameter that is relevant to the photophysical behaviour of imine ligands[16] is the out-of-plane bending (OPB) angle (χ) of the N(imine)–C(aryl) bond with respect to the average plane of the N(imine)-atom of the pyridineimine, the cyclometallated carbons and the iridium atom. Experimental and computed values of −14.1 and −14.3° respectively are found. Closely related information is the dihedral angle, τ, defined by the C(aryl)–N(imine)–Ir–C(*cis* to imine). It amounts to −13.4 and −12.2° for the experimental and computed data respectively. The other compounds show comparable trends and their optimized coordinates are reported in the ESI (Table S9†).

Phenylimine conformational behaviour

We have recently shown[9] that even a large 2-pyrenyl substituent on the imine nitrogen atom does not prevent some degree of torsional freedom of the aromatic moiety around the N–C(aryl) bond. Since the conformational behaviour of the phenyl imine ligand might be relevant to the photophysical behaviour of the complex a detailed study of torsional potential in the ground and first triplet excited state have been also undertaken in the case of **4a**.

The computed torsional energetic profile of S_0 shows another minimum exists which is more stable than the one found in the solid state by 0.91 kcal mol^{-1} (Fig. 4) where the aryl moiety has a torsion angle of −40.4°

The rotation of the aryl substituent around the N–C bond also involves the out-of-plane bending of the carbon atom bonded to the imine nitrogen atom such that the pyramidalization of the nitrogen atom inverts and τ changes from −12.2 to +7.8°.

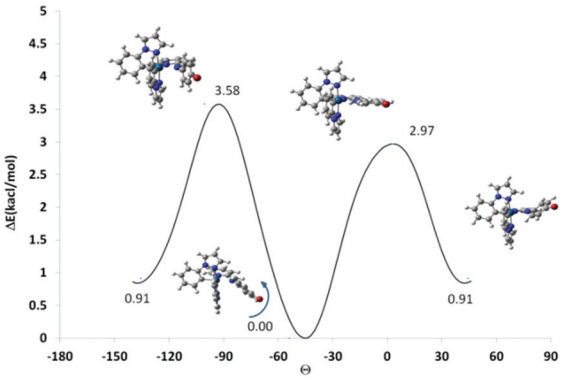

Fig. 4 The computed torsional energetic profile of S_0 for **4a** in DCM.

Electrochemistry

For cationic Ir(III) complexes $[Ir(C\hat{}N)_2(XY)]^+$, the pure metal-centred oxidation is reversible but it becomes less reversible as the contribution of the cyclometallating phenyl(s) to the HOMO increases.[2c,6] The electrochemical properties of **4–8** were examined using cyclic voltammetry (Table 2) and have also been modelled by DFT which shows good agreement with the experimental values (see Fig. 5).

Table 2 Electrochemical data[a] for **4–8**

Entry	Complex	Imine substituent	$E^{1/2}_{Ox}$	$E^{1/2}_{Red1}$	$E^{1/2}_{Red2}$	$\Delta E^{1/2}$ (V)
1	**4a**	(p-C_6H_4Br)	1.41	−0.93	−1.55[b]	2.34
2	**4b**	(p-C_6H_4Br)	1.28	−0.93	−1.54[b]	2.21
3	**4c**	(p-C_6H_4Br)	1.28	−0.95	−1.60[b]	2.23
4	**5a**	Ph	1.39	−0.99	−1.60[b]	2.38
5	**6a**	(p-$C_6H_4CO_2H$)	1.41	−0.87		2.28
6	**7a**	(p-C_6H_4OH)	1.28	−1.06		2.34
7	**8a**	(^{i}Pr)	1.38	−1.25		2.63
8	**[Ir(ppz)$_2$(bipy)][PF$_6$]**		1.37	−1.38		2.75

[a] In dry acetonitrile (0.1 mol L^{-1} of Et_4NClO_4), scan rate 100 mV s^{-1}, all potentials are referenced *vs.* SCE using ferrocinium/ferrocene as an internal standard against a Ag wire (Cp_2Fe^+/Cp_2Fe *vs.* SCE = +0.42 V). [b] Irreversible wave.

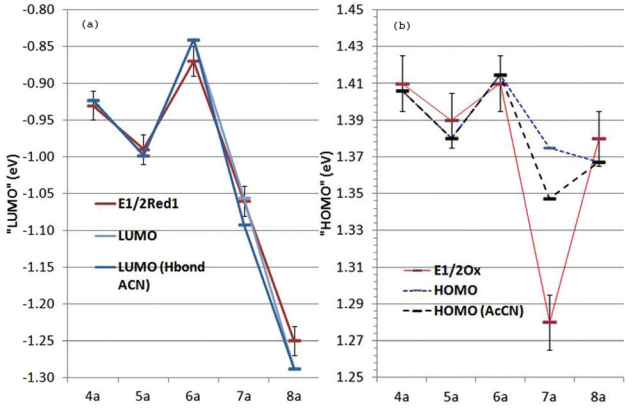

Fig. 5 (a) Experimental reduction potentials and calculated LUMO energies for **4a–8a**, (b) experimental oxidation potentials and calculated HOMO levels for **4a–8a**.

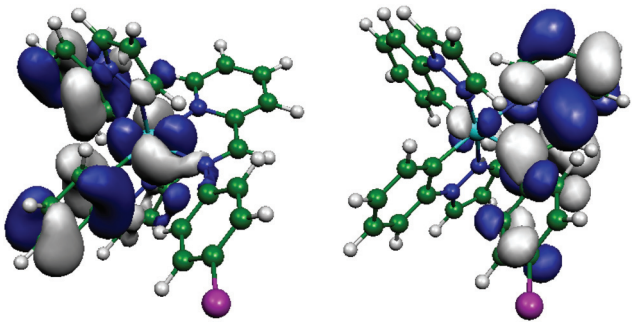

Fig. 6 Calculated HOMO left and LUMO right for **4a**.

All the complexes **4–8** exhibit a reversible/quasi-reversible oxidative process between 1.27 and 1.41 V and a reversible reduction couple between −0.85 and −1.25 V. The relatively small range of oxidation potentials (~0.14 V) suggests that the ionized "orbital" does not have a significant contribution from the pyridineimine ligand. The HOMO and LUMO for **4a** are shown in Fig. 6 those for **5a–8a** are in the ESI (Fig. S4†). The HOMO's of **4a–8a** all involve the Ir atom and the two phenylpyrazole ligands and only partially the Ir–N sigma bond of the imine consistent with other cationic Ir(III) complexes.[2c]

Oxidation of **5a** (R = Ph) occurs at 1.39 V very similar to that, 1.37 V in $[Ir(ppz)_2(bipy)]PF_6$. Comparing complexes **4a–c**, introducing an electron donating Me-substituent(s) on the C^N ligand either *para* to the metal (**4b**)[14] or on the pyrazole (**4c**) makes the complexes easier to oxidise as expected, but has very little effect on the reduction potentials (Table 2, entries 1–3).

The reduction potentials span a wider range (~ 0.40 V) than the oxidation potentials, which suggests that substitution on the pyridineimine ligand mainly affects the reduction, and is consistent with the reduction being mainly pyridineimine based similar to $[Ir(C^N)_2(bipy)]^+$ complexes discussed in the literature.[2c] This is supported by the DFT calculations which show that the LUMO is always mainly localized on the pyridineimine ligand (see Fig. 6 and ESI, Fig. S4†). However, because a pyridineimine is a better π-acceptor than bipyridine the reduction potentials are less cathodic, thus, reduction of **5a** occurs at −0.99 V whereas that of $[Ir(ppz)_2(bipy)]PF_6$ occurs at −1.38 V. In addition, some complexes, also exhibit an irreversible second reduction about 0.6 V more cathodic between −1.55 and −1.60 V. Consistent with that, DFT calculations show that the LUMO+1 is about 0.6 eV higher in energy than the LUMO and is almost completely localized on the pyridine. In comparison, no second reduction potentials were observed in bipyridine complexes of the same cyclometallated ligands.[2c,14]

Introducing electron withdrawing substituents (Br **4a**, CO_2H **6a**) on the *para* position of the *N*-aryl ring of the pyridineimine ligand makes the complexes easier to reduce (by 0.05 to 0.1 V) compared to the N–Ph complex **5a**. In contrast, complex **7a** (R = *p*-C_6H_4OH) is harder to reduce suggesting the positive conjugative effect of OH outweighs the negative inductive effects. Somewhat surprisingly **7a** is easier to oxidise than **5a** (by 0.1 V). This effect is reproduced, though to a lesser extent by DFT computations. On the other hand adding an explicit MeCN molecule H-bonded to the hydrogen atom of the OH group there is a significant improvement in modelling the oxidation potential and a small one in the reduction potential. This finding suggests that H-bonding may play a significant role in this case. Upon changing the pyridineimine substituent from Ph group **5a** to iPr **8a** the oxidation potential is unaffected, however, the reduction potential of the latter is considerably more cathodic (0.26 V). Since the LUMO is localised on the π orbital of the pyridineimine replacement of Ph by iPr reduces the delocalization within this ligand and increases the π-orbital energy and hence gives rise to an even more cathodic reduction potential. Thus, altering the substituent on the imine N can tune the reduction potential by almost 0.4 V whilst having very little effect on the oxidation potentials.

Photophysical properties

The data from the UV-vis absorption spectra for complexes **4–8a** are shown in Table 3 (absorption, emission and excitation

Table 3 Photophysical data in CH_2Cl_2

Entry	Complex	λ_{abs} [nm] (ε_{max} [dm^3 mol^{-1} cm^{-1}])	λ_{em}[a] [nm]	QY[b] (%)
1	**4a**	236 (27 750), 330 (9690), 508 (400)	730	0.06
2	**4b**	241 (19 300), 339 (6580), 526 (180)	760	0.04
3	**4c**	247 (17 800), 339 (5670), 547 (160)	780	0.06
4	**5a**	235 (58 100), 325 (19 400), 506 (100)	715	0.33
5	**6a**	241 (14 560), 326 (5020), 521 (90)	735	0.49
6	**7a**	244 (24 150), 326 (6360), 375 (7640), 511 (240)	735	0.06
7	**8a**	255 (27 000), 323 (6500), 473 (60)	640	6

[a] Emission spectra under N_2 or argon and have been corrected for photomultiplier response. [b] Quantum yields were measured relative to **8a** by decomposing the spectra and then integrating the decomposing functions. It should be borne in mind that the aryl complexes are only weakly emissive and in a range where the photomultiplier response is weak therefore there is a significant error in these measurements. The quantum yield of **8a** was measured using an integrating sphere in argon saturated solution.

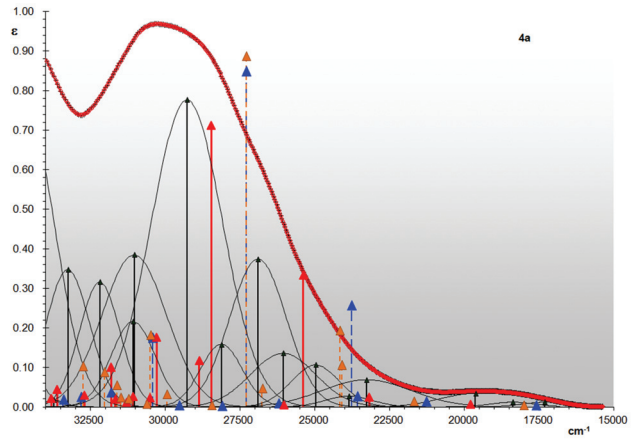

Fig. 7 Low energy (270–650 nm) part of the absorption spectra of **4a**. (▲) Position of fitting Gaussian functions; TD-DFT computed intensities and wavenumbers for **4a** and (▲) PF_6^- on the phenylpyrazole side (**4a**-PF6PZ) and (▲) PF_6^- on the phenylimine side (**4a**-PF6PI). (▲) **4a** cation (see Fig. S8 in ESI† for **5a** and **8a**).[21]

spectra are provided in the ESI, Fig. S5a–c†) and those for representative compounds **4a**, **5a**, and **8a**[17] have been analysed by decomposing in Gaussian functions[18] in order to facilitate comparison to the computational results as illustrated in Fig. 7 for **4a**. A detailed TD-DFT study has then been performed for these representative compounds **4a**, **5a** and **8a**.

Decomposition of the most intense absorption bands in the range 230–270 nm (43 000–32 000 cm^{-1}), showing only very moderate features, is the result of four or five Gaussian functions with large intensity (see Table S3 and Fig. S6 in ESI†). According to the TD-DFT calculations this band is the envelope of many closely spaced transitions of moderate intensity which are assigned to the spin allowed multideterminantal inter- and intra-ligand IL ($\pi \rightarrow \pi^*$) transitions although in some cases some of the configurations involve molecular orbitals with a non-negligible contribution from metal d-orbitals (see for example orbital #160 for **4a** in ESI Fig. S9†).

For the moderately intense absorption band in the range 270–440 nm (*i.e.*, 32 000–22 500 cm^{-1}) decomposition suggests that it is mainly due to the three most intense Gaussian functions that fall at around 31 000 (320 nm), 29 000 (340 nm) and 26 500 cm^{-1} (370 nm) (31031, 29 268 and 26 892, cm^{-1} for **4a**) and some further contributions of small intensity. Similar description can be given for the other compounds **5a**, and **8a** (Table S3 in ESI†).

TD-DFT calculations of the "free" cation in the gas phase gave very poor agreement with the experimental data in this region, irrespective of the basis set and exchange correlation functional used. Introducing the contribution from the dichloromethane solvent by means of the Self Consistent Reaction Field approach[19] reduced the disagreement but was still unable to describe the features suggested by the decomposition procedure. Recently the effect of ion pairing on absorption spectra has been reported to give better agreement between calculated and experimental absorption spectra for some related cyclometallated iridium complexes.[20] Hence, the effect of the anion was modelled, the two most stable ion pairs were considered, *i.e.* the cation with the PF_6^- close to the pyridineimine side of the molecule (**4a**-PF6PI) and with the anion close to the phenylpyrazole side (**4a**-PF6PZ) (see Fig. S7† in ESI for their optimized structures and energies). This approach shows a far better agreement with the experimental data and suggests that these three species, the free cation and two ion pairs, contribute to the experimental spectra (see ESI† for more discussion).

TD-DFT calculations (Table 4) suggest that the lowest energy part of the spectrum, in the range 320–650 nm (31 250–15 380 cm^{-1}) is due to two very low intensity transitions. These are S_1 and S_2 which are almost pure HOMO → LUMO and (HOMO−2) → LUMO excitations respectively. For **4a**, **5a** and **8a** the uniform composition of the involved MO's in terms of atomic orbitals suggests these transitions can be described as spin allowed metal + ligand to other-ligand charge transfer [dπ (Ir) + π C^N] → π* (X^Y), *i.e.*, broadly (^{1}MLL'CT). Some further transitions due to spin forbidden $S_0 \rightarrow T_n$ excitations might give contributions in different regions of the spectrum in particular close to spin allowed transitions involving MO's with large weight of metal d-orbitals.

Preliminary experiments showed that all of the pyridineimine complexes **4–8** emit in solution (CH_2Cl_2) at room temperature (Fig. 8 and Fig. S5b in ESI†). The aryl complexes in particular emit at long wavelength, towards the NIR, however the emission intensity is rather weak for these complexes. Because the excitation spectra (see Fig. S5c in ESI†) look similar for all the complexes the same excitation wavelength (390 nm) was used in all cases. The complexes all show one broad emission band at 640–740 nm (Table 3). The quantum yields relative to the isopropyl complex **8a** are shown in Table 3, the aryl complexes are much weaker emitters than the isopropyl complex. The isopropyl complex **8a** showed an observed lifetime of 145 ns in argon saturated solution and 100 ns in air. The lifetime suggests a triplet contribution to the emission as does the significant reduction of intensity in the presence of air.

Putting electron donating methyl substituent(s) on the C^N ligand either *para* to the metal **4b** or on the pyrazole **4c** results in a considerable red shift from 730 nm for **4a** to 760 and 780 nm for **4b** and **4c** respectively. This is consistent with the electrochemical data, which show an easier oxidation (raised HOMO) for these complexes. Complexes with the electron withdrawing *N*-aryl substituents on the pyridineimine (**4a** *p*-Br, **6a** *p*-CO_2H) are red shifted compared to **5a** (R = H) though in these cases the shift is due to a lowering of the LUMO consistent with the easier reduction. An OH substituent also gives a small red shift in the emission wavelength. Replacing the *N*-aryl substituent on the imine with an isopropyl leads to a significant blue shift to 640 nm, compared to 715 nm for **5a** consistent with the higher LUMO (more cathodic reduction) of **8a**.

The results suggest that the emission always starts from excited states which are strongly influenced by the HOMO and/or LUMO energies and that are probably the lowest excited

Table 4 Computed electronic transitions at D95(d))/SDD/M06/DCM level of theory for **4a–8a** (data for the ion pairs is in the ESI Tables S4–7)

	4a		**5a**		**8a**	
	λ (nm) $\tilde{\nu}$ (cm^{-1}) (f)	Excitation MOs (contribution %)	λ (nm) $\tilde{\nu}$ (cm^{-1}) (f)	Excitation MOs (contribution %)	λ (nm) $\tilde{\nu}$ (cm^{-1}) (f)	Excitation MOs (contribution %)
1	555 18 020 (0.0019)	HOMO → LUMO (0.98)	544 18 388 (0.0016)	HOMO → LUMO (0.98)	497 20 105 (0.0001)	HOMO → LUMO (0.97)
2	461 21 687 (0.0056)	HOMO−3 → LUMO (0.03) HOMO−2 → LUMO (0.95)	453 22 077 (0.0045)	HOMO−3 → LUMO (0.04) HOMO−2 → LUMO (0.94)	422 23 691 (0.0002)	HOMO−2 → LUMO (0.98)
3	415 24 088 (0.0427)	HOMO−3 → LUMO (0.17) HOMO−1 → LUMO (0.82)	408 24 489 (0.1185)	HOMO−3 → LUMO (0.94) HOMO−2 → LUMO (0.03)	381 26 267 (0.0769)	HOMO−3 → LUMO (0.67) HOMO−1 → LUMO (0.31)
4	414 24 164 (0.0774)	HOMO−5 → LUMO (0.02) HOMO−3 → LUMO (0.75) HOMO−1 → LUMO (0.18)	407 24 558 (0.006)	HOMO−1 → LUMO (0.99)	379 26 382 (0.0397)	HOMO−3 → LUMO (0.30) HOMO−1 → LUMO (0.67)
5	374 26 758 (0.0187)	HOMO−4 → LUMO (0.94)	367 27 229 (0.0058)	HOMO−4 → LUMO (0.96)	343 29 117 (0.0006)	HOMO−4 → LUMO (0.97)
6	366 27 294 (0.3547)	HOMO−6 → LUMO (0.39) HOMO−5 → LUMO (0.51) HOMO−4 → LUMO (0.04) HOMO−3 → LUMO (0.03)	354 28 216 (0.2469)	HOMO−6 → LUMO (0.91) HOMO−5 → LUMO (0.03)	331 30 198 (0.0006)	HOMO → LUMO+1 (0.94)
7	352 28 442 (0.0021)	HOMO−6 → LUMO (0.56) HOMO−5 → LUMO (0.43)	347 28 847 (0.002)	HOMO−6 → LUMO (0.03) HOMO−5 → LUMO (0.94)	328 30 515 (0.0823)	HOMO → LUMO +2 (0.91)

f = oscillator strength.

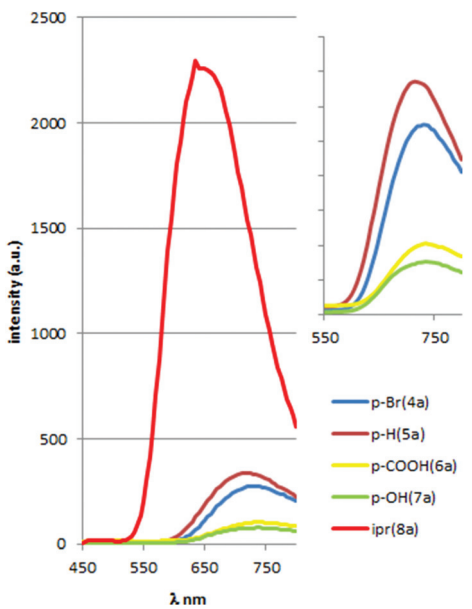

Fig. 8 Emission spectra for approximately equimolar solutions of **4a–8a**. Inset expansion of aryl complexes **4a–7a**.

triplet states in agreement with the "Kasha Rule". We have undertaken a detailed study of the triplet excited states for **4a**, **5a**, **8a** and their PF6PI ion pairs which are considered representative of all the complexes **4–8**. Furthermore for **4a**, **5a**, and **8a** the substituent on the imine is unlikely to have specific (*e.g.*, H-bond) interactions with the solvent.

Since some doubt has been cast[22] on the reliability of the TD-DFT triplet energies the triplet structures have been energy minimized using the variational UKS approach for all three compounds. The S_0–T_1 energy difference computed as ΔSCF energy where T_1 UKS and the S_0 structures are at the S_0 ($\Delta E(T_1@T_1{:}S_0@S_0)$ and T_1 ($\Delta E(T_1@T_1{:}S_0@T_1)$) relaxed geometry are reported in Table 5, column a and b. The former are too "blue" compared to the experimental values showing a clear effect of the ground state structure relaxation on the emission energy. On the other hand using for the ground S_0 state the relaxed triplet geometry (*i.e.* vertical emission) the computed wavelength values are 921, 832 and 682 nm. Although the relative trend of the computed wavelengths is still in the correct order (**4a** > **5a** > **8a**) and the value of **8a** is in reasonable agreement with the experimental one, those of **4a** and **5a** are in large disagreement.

The observed emission intensity from the excited state Ψ_κ to the ground state singlet Ψ_0 has two main contributions: one from the spin–orbit coupling that mixes the pure singlet and pure triplet states and one due to both the geometry and the vibrational modification following the electronic reorganization in the two different electronic states that can be taken

Table 5 ΔE(T1→S0) computed at the unrestricted DFT SDD/D95(d)/M06/DCM level of theory

	ΔSCF		Exp
	a	b	
4a	666	921	780
4a M062X		748	
5a	638	832	715
5a M062X		718	
8a	564	682	640
8a M062X		586	

[a] T_1 at T_1 relaxed geometry, S_0 at ground state geometry(T_1@T_1:S_0@S_0). [b] T_1 and S_0 calculated at relaxed T1 geometry(T_1@T_1:S_0@T_1). For values for ion pairs see ESI Table S8.

into account by the Franck-Condon factors. These modifications include also the counter ion in the case of ion pair. If the M062X xc-functional is used, that takes better account of the effect of charge separation including a large contribution of the Hartree–Fock exchange, then agreement for the aryl compounds is significantly better though the isopropyl wavelength is now too blue. We note that decomposition of the broad emission band of **8a** (see Fig. S11†) suggests there are two contributions a major one from the free cation and a lesser one from the ion pair (see ESI for further discussion).

There is a large difference in the quantum yields of the studied *N*-aryl derivatives (**4a–7a**) compared to the *N*-alkyl **8a** (**8a** is at least 10 times as intense see Table 3) that cannot easily be justified by a different spin–orbit contribution. For **4a–8a** and their ion pairs the coefficients of the d orbital of the MO's involved in the transition are very similar hence changes in spin–orbit coupling do not justify the observed large difference in emission intensity even among the "free" cations. On excitation different internal degrees of freedom can be modified, rotation of the *N*-aryl substituent in the ground state has already been discussed (Fig. 4), in addition, change of the geometry around the imine nitrogen atom can cause significant changes in the coordination of the pyridineimine ligand.[2,3] This can lead to large differences in the equilibrium geometries in the S_0, S_1 and T_1 states particularly evident in the "out of plane" bending (OPLB) of the N–C(aryl) bond allowing the Franck-Condon factors to further modulate the emission intensity. Analysis of the molecular geometry of the S_0, S_1 and T_1 states in case of aryl (**4a**, **5a**) and alkyl (**8a**) substituted imine illustrates a striking difference between the two kinds of molecule both in case of the free cation (Fig. 9), and the ion pairs (see ESI, Fig. S10†).

The "out of plane" bending of the N(im)–C(aryl) bond is defined by the dihedral angle between the planes identified by the atoms C(im)–Ir–N(im) (light blue) and Ir–N(im)–C(aryl/alkyl) (red). The dihedral is positive if the rotation looking from the C(im) atom toward the Ir atom is clockwise for superimposing the "light blue" to the "red plane".

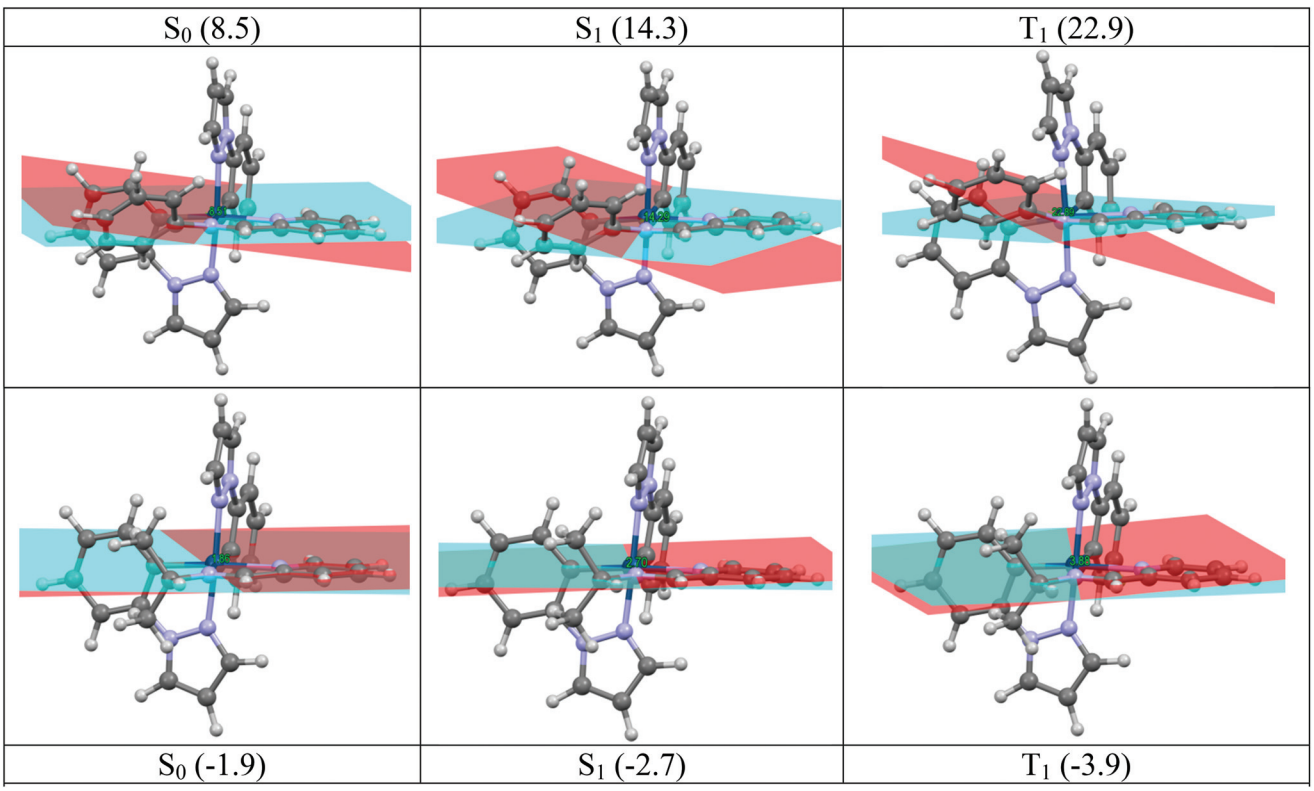

Fig. 9 Minimum energy structures of **5a** (above) and **8a** (below) in the ground (S_0), first singlet (S_1) and first triplet state (T_1) computed at the D95/SDD/M06/DCM level of theory. The angle between the planes is shown in parentheses.

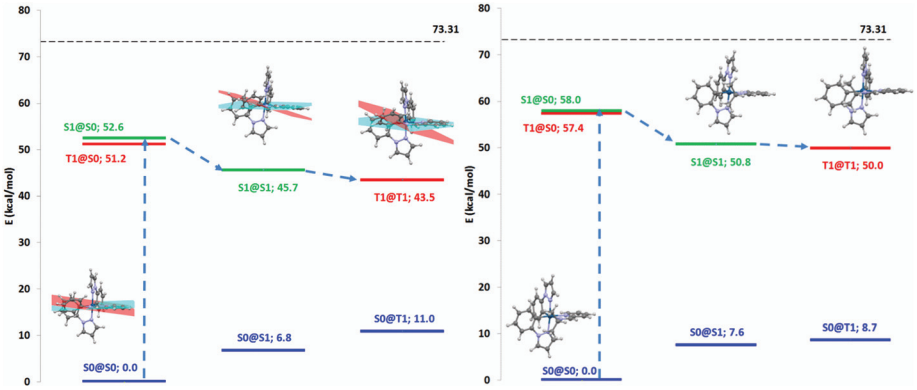

Fig. 10 Energies of S_0 (blue), S_1 (green) and T_1 (red) states at their relaxed and unrelaxed geometries and their optimized structures for **5a** (left) and **8a** (right). The black line (73.31 kcal mol^{-1}) corresponds to the excitation energy.

In the case of **5a** the ground state S_0, S_1 and T_1 have minimum energy equilibrium geometries characterized by angles ϕ of 8.5, 14.3 and 22.9° respectively, hence the geometry of the first triplet excited state (Fig. 10) is considerably different than in the ground state reducing the FC factors. Similar behaviour is shown by the other aryl derivative **4a**. On the other hand in case of **8a** the angles are −1.9, −2.7, and −3.9° respectively and the ground and T_1 states have closer equilibrium geometries as in case of **8a** so these effects are not very relevant. Similar values are found if the ion pairs are considered (see ESI Fig. S10†).

Furthermore the geometry of the S_1 and the T_1 states are closer in **8a** than in the corresponding states of **5a** making the ISC process easier for **8a**. In summary aryl-substituted pyridineimines incur more difficult $S_1 \rightarrow T_1$ and $T_1 \rightarrow S_0$ ISC processes than alkyl-substituted ones reducing the emission intensity of aryl-substituted complexes.

Conclusions

In conclusion we have demonstrated that the use of pyridineimines in place of bipyridine in biscyclometallated iridium complexes leads to complexes that are easier to reduce and which emit at longer wavelengths. The longer wavelength emission might make these complexes particularly suited to biological applications. Variation in the substituent on the imine leads to changes in emission wavelength that are consistent with the electrochemical properties. DFT calculations provide evidence for excited state geometry changes in aryl-substituted pyridineimines which lead to significant loss in emission intensity. The pyridineimine complexes are easy to prepare, particularly since the pyridineimine ligand can be prepared *in situ* from pyridine carboxaldehyde and the relevant amine. The ready availability of a wide range of amines with additional functionality means that further modification of the complexes *e.g.* bioconjugation, should be relatively easy.

Experimental

Materials and methods

All reactions were carried out under an inert atmosphere of nitrogen and under microwave irradiation unless stated otherwise. After work up all the complexes were air-stable. Microwave reactions were carried out in a *CEM-Discover* commercial microwave reactor. ^1H, and $^{13}C\{^1H\}$ NMR spectra were obtained using a DRX 400 MHz spectrometer. Chemical shifts were recorded in ppm (on δ scale with tetramethylsilane as internal reference), and coupling constants are reported in Hz. The labelling for NMR assignments is shown in the ESI.† FAB mass spectra were obtained on a Kratos concept mass spectrometer using NOBA as matrix. The electrospray (ES) mass spectra were recorded using a micromass Quattra LC mass spectrometer in HPLC grade acetonitrile. UV-Vis absorption measurements were carried out on a Shimadzu UV-1600 series spectrometer in dry DCM. Luminescence studies were performed in dry DCM using a Jobin Yvon Horiba Fluoromax-P spectrofluorimeter. For emission measurements, all complexes were excited at a wavelength of 390 nm using a filter of 450 nm. Electrochemical measurements were performed with an Eco Chemie Autolab. All measurements were carried out in a one-compartment cell under N_2 gas, equipped with a Pt disc working electrode, a Pt gauze counter electrode and a silver wire reference electrode. The supporting electrolyte was Et_4NClO_4 (0.1 mol L^{-1}) in acetonitrile. Elemental analyses were performed at London Metropolitan University. All starting materials were obtained from Aldrich or Alfa Aesar.

Computational details

The decomposition of the absorption spectra was a non-linear fitting of a set of Gaussian functions (see ref. 16). DFT computations were applied by using the meta-hybrid xc functional M06[24] as implemented in the Gaussian 09 suite of programs[25] that has been shown to be effective in dealing with similar complexes.[26] Some preliminary calculations were performed using the modified Perdew–Burke–Ehrzenov functional.[27] Geometry optimizations were performed using the Dunning/

Huzinaga double-ζ (D95) basis sets,[28] adding a set of polarization functions to the same basis set in case of C, N, P, F atoms. The Stuttgart/Dresden ECP basis set and pseudopotential for small core taking into account relativistic effects were used for Ir and Br.[29] Default gradient and displacement thresholds were used for the geometry optimization convergence criteria. The dichloromethane (DCM) and acetonitrile (ACN) solvents environment were modelled according to the SCRF model.[30] To confirm that the obtained geometries are relative minima on the molecular energy hypersurface, analytical computation of the Hessian matrix with respect to the nuclear coordinates at the same level of theory was performed. The programs Molekel4.3[31] and Mercury CSD 2.0[32] were used to draw chemical structures and orbital composition.

Time dependent DFT were computed using the same exchange correlation functional. Calculations were performed for both the cation in solution and in gas phase. Furthermore the ion pairs with the PF_6 were optimized starting from the geometry of the crystal structure. Excited states for the calculation of the absorption spectra were computed using the optimized geometries of the singlet ground state (vertical excitation). The structure of the first triplet state has been computed using the unrestricted wavefunction (UKS) within the Kohn-Sham DFT.

The Hessian of the computed wavefunction has been checked against possible internal instability.[33] Emission energies were computed also as the difference (so called ΔSCF) between the UKS molecular energy of the triplet state at the relaxed geometry of the triplet state and the energy of the singlet ground state at the triplet geometry (vertical de-excitation).

General procedure for synthesis of [Ir(C^N)$_2$(pyridineimine)][PF$_6$] (4–9)

The appropriate dimer, $[Ir(C^N)_2Cl]_2$, pyridine-2-carboxaldehyde (2.4 equiv.), KPF_6 (2–2.4 equiv.) and the relevant amine (2.4 equiv.) were placed in a microwave vial and the solvent (3 ml) was added. Nitrogen was bubbled through the solution for 2 min and the vial was then sealed with a septum cap. The tube was placed in the microwave reactor and heated under microwave irradiation. After this time the solvent was removed *in vacuo* leaving behind a solid which was dissolved in DCM (15 ml) and passed through celite. The filtrate was reduced in volume and hexane was added slowly to induce precipitation. The precipitate was isolated, washed with hexane and dried *in vacuo.* The compounds could be recrystallised from DCM–hexane. Early attempts were carried out at 100 °C for 30 min in ethanol but later milder conditions (20 min at 60 °C in methanol) were found to work just as well. Hence the reactions are done under the milder conditions unless stated otherwise. In the mass spectrometry data $[M]^+$ will refer to just the complex cation.

Synthesis of 4a. This was prepared from dimer **3a** (50 mg, 0.049 mmol), 4-bromoaniline (20.3 mg, 0.118 mmol), pyridine–2-carboxaldehyde (12.7 mg, 12 μL, 0.118 mmol) and KPF_6 (18.1 mg, 0.098 mmol) and after work up gave **4a** as a red solid (74 mg, 86%). Anal. Calcd for $C_{31}H_{25}BrCl_2F_6IrN_6P$: C, 38.40, H, 2.60, N, 8.67. Found: C, 38.46, H, 2.51, N, 8.62%. ^{1}H NMR ($CDCl_3$): δ 9.33 (1H, s, H_5), 8.52 (1H, bd, J = 7.4, H_4), 8.09 (2× overlapping 1H, td, J = 7.4, 1.5, H_3, d, J = 2.0, H_e), 8.02–8.01 (2H, m, $H_{1,\ e'}$), 7.53 (1H, d, J = 2.3, H_g), 7.46 (1H, ddd, J = 7.8, 5.5, 1.2, H_2), 7.27 (1H, dd, J = 7.8, 1.2, H_d), 7.23–7.19 (2H, m, $H_{7,\ 7'}$), 7.07 (1H, dd, J = 7.8, 1.2, $H_{d'}$), 7.05 (1H, td, J = 7.8, 1.2, H_c), 6.95 (1H, d, J = 2.3, $H_{g'}$), 6.90–6.84 (4H, m, $H_{6,\ 6',\ b,\ c'}$), 6.70 (1H, td, J = 7.8, 1.2, $H_{b'}$), 6.65 (1H, t, J = 2.5, H_f), 6.61 (1H, t, J = 2.5, $H_{f'}$), 6.25 (1H, dd, J = 7.4, 1.2, H_a), 6.05 (1H, dd, J = 7.4, 1.2, $H_{a'}$). ^{13}C NMR: 169.14 (C_5), 156.29 (C_{10}), 150.40 (C_1), 146.58 (C_9), 142.33 (C_h), 142.02 ($C_{h'}$), 139.75 (C_3), 139.70 (C_g), 138.55 ($C_{g'}$), 133.26 ($C_{a'}$), 133.07 (C_a), 132.09 ($C_{7,\ 7'}$), 131.61 (C_4), 131.14 ($C_{i'}$), 130.23 (C_i), 129.06 (C_2), 127.03 (C_b), 126.69 ($C_{b'}$), 126.62 (C_e), 126.55 ($C_{e'}$), 124.07 ($C_{6,\ 6'}$), 123.70 (C_c), 123.15 ($C_{c'}$), 123.06 (C_8), 111.59 (C_d), 111.18 ($C_{d'}$), 108.80 (C_f), 108.58 ($C_{f'}$). MS (FAB): m/z 739 $[M]^+$.

Synthesis of 4b. This was prepared from dimer **3b** (60 mg, 0.055 mmol), 4-bromoaniline (22.7 mg, 0.132 mmol), pyridine–2-carboxaldehyde (14.2 mg, 12.6 μL, 0.132 mmol) and KPF_6 (24.3 mg, 0.132 mmol) and after work up gave **4b** as a red solid (82 mg, 82%). Anal. Calcd for $C_{32}H_{27}BrF_6IrN_6P$: C, 42.11, H, 2.98, N, 9.21. Found: C, 42.17, H, 3.03, N, 9.28%. ^{1}H NMR (CD_2Cl_2): δ 9.21 (1H, s, H_5), 8.38 (1H, dd, J = 7.8, 1.2, H_4), 8.16–8.10 (3H, m, $H_{1,\ 3,\ e}$), 8.06 (1H, dd, J = 3.1, 0.8, $H_{e'}$), 7.52 (1H, ddd, J = 7.8, 5.5, 1.6, H_2), 7.46 (1H, d, J = 2.3, H_g), 7.30–7.26 (2H, m, $H_{7,\ 7'}$), 7.16 (1H, s, H_d), 6.98 (1H, s, $H_{d'}$), 6.88 (1H, d, J = 2.3, $H_{g'}$), 6.86–6.82 (2H, m, $H_{6,\ 6'}$), 6.72 (1H, dd, J = 7.8, 0.8, H_b), 6.63 (1H, t, J = 2.7, H_f), 6.60–6.56 (2H, m, $H_{b',\ f'}$), 6.09 (1H, d, J = 7.8, H_a), 5.93 (1H, d, J = 7.8, $H_{a'}$), 2.32 (3H, s, Me), 2.24 (3H, s, Me′). ^{13}C NMR: 168.90 (C_5), 156.38 (C_{10}), 151.55 (C_1), 147.21 (C_9), 142.79 (C_h), 142.53 ($C_{h'}$), 140.02 (C_3), 139.90 (C_g), 138.65 ($C_{g'}$), 134.02 (C_c), 133.36 ($C_{c'}$), 133.28 ($C_{a'}$), 132.93 (C_a), 132.47 ($C_{7,\ 7'}$), 131.22 (C_4), 129.93 (C_2), 128.18 (C_f), 127.83 ($C_{f'}$), 127.39 (C_e), 127.26 ($C_{e'}$), 127.17 ($C_{i'}$), 126.06 (C_i), 124.50 ($C_{6,\ 6'}$), 123.33 (C_8), 113.05 (C_d), 112.61 ($C_{d'}$), 108.87 (C_f), 108.70 ($C_{f'}$), 21.11 (Me), 21.03 (Me′). MS (FAB): m/z 767 $[M]^+$.

Synthesis of 4c. This was prepared from dimer **3c** (50 mg, 0.044 mmol), 4-bromoaniline (18.2 mg, 0.106 mmol), pyridine–2-carboxaldehyde (11.3 mg, 10.1 μL, 0.106 mmol) and KPF_6 (19.5 mg, 0.106 mmol) and after work up gave **3c** as a red solid (73 mg, 89%). Anal. Calcd for $C_{34}H_{31}BrF_6IrN_6P$: C, 43.41, H, 3.32, N, 8.93. Found: C, 43.35, H, 3.36, N, 8.84%. ^{1}H NMR (CD_2Cl_2): δ 9.20 (1H, s, H_5), 8.39 (1H, dd, J = 7.8, 0.8, H_4), 8.13 (1H, td, J = 7.8, 1.6, H_3), 7.98 (1H, ddd, J = 5.4, 1.6, 0.8, H_1), 7.53–7.49 (2H, m, $H_{2,\ d}$), 7.22–7.18 (2H, m, $H_{7,\ 7'}$), 7.10 (1H, dd, J = 8.2, 1.2, $H_{d'}$), 7.06 (1H, ddd, J = 8.2, 7.4, 1.6, H_c), 6.91 (1H, ddd, J = 8.2, 7.4, 1.6, $H_{c'}$), 6.81 (1H, td, J = 7.4, 0.8, H_b), 6.78–6.73 (3H, m, $H_{6,\ 6',\ b'}$), 6.35 (1H, dd, J = 7.4, 1.6, H_a), 6.21 (1H, dd, J = 7.8, 1.6, $H_{a'}$), 6.14 (1H, s, H_f), 6.06 (1H, s, $H_{f'}$), 2.84 (3H, s, Me_B), 2.56 (3H, s, $Me_{B'}$), 2.13 (3H, s, Me_A) 1.56 (3H, s, $Me_{A'}$). ^{13}C NMR: 167.98 (C_5), 156.55 (C_{10}), 151.19 (C_1), 150.69 (C_g), 150.09 ($C_{g'}$), 146.53 (C_9), 144.72 ($C_{i'}$), 144.54 (C_i), 142.16 (C_e), 141.71 ($C_{e'}$), 139.82 (C_3), 133.92 (C_a), 133.84 ($C_{a'}$), 132.67 ($C_{h'}$), 132.13 ($C_{7,\ 7'}$), 131.19 (C_4), 130.61 (C_h), 130.18 (C_2),

125.98 (C_b), 125.81 ($C_{b'}$), 124.76 ($C_{6,\ 6'}$), 123.99 (C_c), 123.55 ($C_{c'}$), 123.40 (C_8), 113.23 (C_d), 112.83 ($C_{d'}$), 110.56 ($C_{f'}$), 110.44 (C_f), 14.76 (Me_B), 14.45 ($Me_{B'}$), 14.07 (Me_A), 12.47 ($Me_{A'}$). MS (FAB): m/z 795 $[M]^+$.

Synthesis of 5a. This was prepared from dimer **3a** (50 mg, 0.049 mmol), aniline (11 mg, 10.8 μL, 0.118 mmol), pyridine–2-carboxaldehyde (12.7 mg, 12 μL, 0.118 mmol) and KPF_6 (18.1 mg, 0.098 mmol) and after work up gave **5a** as a red solid (58 mg, 75%). Anal. Calcd for $C_{30}H_{24}F_6IrN_6P$: C, 44.72, H, 3.00, N, 10.43. Found: C, 44.81, H, 3.07, N, 10.39%. ^{1}H NMR (CD_2Cl_2): δ 9.19 (1H, s, H_5), 8.36 (1H, bd, J = 7.4, H_4), 8.17–8.07 (4H, m, $H_{1,\ 3,\ e,\ e'}$), 7.54–7.51 (2H, m, $H_{2,\ g}$), 7.34 (1H, bd, J = 8.2, H_d), 7.21–7.06 (5H, m, $H_{7,\ 7',\ 8,\ c,\ d'}$), 6.94–6.85 (5H, m, $H_{6,\ 6',\ b,\ c',\ g'}$), 6.68 (1H, td, J = 7.4, 1.2, $H_{b'}$), 6.65 (1H, t, J = 2.4, H_f), 6.62 (1H, t, J = 2.4, $H_{f'}$), 6.27 (1H, dd, J = 7.4, 1.2, H_a), 6.07 (1H, dd, J = 7.4, 1.2, $H_{a'}$). ^{13}C NMR: 168.55 (C_5), 156.45 (C_{10}), 151.57 (C_1), 148.21 (C_9), 142.90 (C_h), 142.62 ($C_{h'}$), 140.17 (C_3), 140.05 (C_g), 138.71 ($C_{g'}$), 133.66 ($C_{a'}$), 133.40 (C_a), 131.63 ($C_{i'}$), 131.02 (C_4), 130.60 (C_i), 129.89 (C_2), 129.41 ($C_{7,\ 7'}$), 129.36 (C_8), 127.61 (C_e), 127.42 (C_b), 127.30 ($C_{e'}$), 126.77 ($C_{b'}$), 124.17 (C_c), 123.41 ($C_{c'}$), 122.57 ($C_{6,\ 6'}$), 112.24 (C_d), 111.65 ($C_{d'}$), 108.99 (C_f), 108.84 ($C_{f'}$). MS (FAB): m/z 661 $[M]^+$.

Synthesis of 6a. This was prepared from dimer **3a** (100 mg, 0.097 mmol), 4-aminobenzoic acid (32 mg, 0.233 mmol), pyridine-2-carboxaldehyde (25 mg, 22 μL, 0.233 mmol) and KPF_6 (49 mg, 0.233 mmol) and after work up gave **6a** as an orange-brown solid (155 mg, 94%). Anal. Calcd for $C_{31}H_{24}F_6IrN_6O_2P$: C, 43.82, H, 2.85, N, 9.89. Found: C, 43.92, H, 2.79, N, 9.83%. ^{1}H NMR (CD_2Cl_2): δ 9.36 (1H, s, H_5), 8.48 (1H, d, J = 6.6, H_4), 8.16 (1H, d, J = 2.7, H_e), 8.07–8.03 (3H, m, $H_{1,\ 3,\ e'}$), 7.63–7.61 (3H, m, $H_{7,\ 7',\ g}$), 7.47 (1H, dd, J = 7.4, 5.1, H_2), 7.34 (1H, dd, J = 7.8, 0.8, H_d), 7.10–7.06 (2H, m, $H_{c,\ d'}$), 6.94 (1H, d, J = 2.0, $H_{g'}$), 6.88–6.80 (4H, m, $H_{6,\ 6',\ b,\ c'}$), 6.66–6.63 (2H, m, $H_{b',\ f}$), 6.60 (1H, t, J = 2.3, $H_{f'}$), 6.26 (1H, dd, J = 7.8, 1.2, H_a), 6.06 (1H, dd, J = 7.4, 1.2, $H_{a'}$). ^{13}C NMR: 170.23 (C_5), 168.89 (C_{11}), 156.39 (C_{10}), 151.42 (C_1), 151.29 (C_9), 142.91 (C_h), 142.56 ($C_{h'}$), 140.28 (C_3), 140.11 (C_g), 138.84 ($C_{g'}$), 133.59 ($C_{a'}$), 133.36 (C_a), 132.61 (C_8), 131.68 (C_4), 131.47 ($C_{i'}$), 130.90 ($C_{7,\ 7'}$), 130.53 (C_i), 130.01 (C_2), 127.64 (C_b), 127.51 (C_e), 127.23 ($C_{e'}$), 126.83 ($C_{b'}$), 124.16 (C_c), 123.52 ($C_{c'}$), 122.55 ($C_{6,\ 6'}$), 112.24 (C_d), 111.73 ($C_{d'}$), 109.07 (C_f), 108.87 ($C_{f'}$). MS (FAB): m/z 705 $[M]^+$.

Synthesis of 7a. This was prepared from dimer **3a** (40 mg, 0.039 mmol), 4-aminophenol (10.2 mg, 0.094 mmol) and pyridine-2-carboxaldehyde (10.1 mg, 8 μL, 0.094 mmol) and after work up gave **7a** as a red solid (45 mg, 87%). Anal. Calcd for $C_{30}H_{24}ClIrN_6O$: C, 50.59, H, 3.40, N, 11.80. Found: C, 50.62, H, 3.31, N, 11.70%. ^{1}H NMR (MeOD): δ 9.29 (1H, s, H_5), 8.57 (1H, d, J = 3.1, H_e), 8.47 (1H, d, J = 2.3, $H_{e'}$), 8.36 (1H, bd, J = 7.8, H_4), 8.19 (1H, td, J = 7.8, 1.6, H_3), 8.10 (1H, d, J = 5.5, H_1), 7.69 (1H, d, J = 2.3, H_g), 7.59 (1H, ddd, J = 7.8, 5.5, 1.2, H_2), 7.53 (1H, dd, J = 7.8, 1.2, H_d), 7.32 (1H, dd, J = 7.8, 1.2, $H_{d'}$), 7.11 (1H, dd, J = 2.3, 0.8, $H_{g'}$), 7.06 (1H, td, J = 7.8, 1.2, H_c), 6.91–6.87 (3H, m, $H_{6,\ 6',\ c'}$), 6.84 (1H, td, J = 7.4, 1.2, H_b), 6.71 (1H, t, J = 2.3, H_f), 6.69 (1H, m, $H_{b'}$), 6.67 (1H, t, J = 2.3, $H_{f'}$), 6.51–6.47 (2H, m, $H_{7,\ 7'}$), 6.26 (1H, dd, J = 7.8, 1.2, H_a), 6.09 (1H, dd, J = 7.4, 1.2, $H_{a'}$). ^{13}C NMR: 166.03 (C_5), 158.64 (C_8), 156.84 (C_{10}), 150.60 (C_1), 142.85 (C_h), 142.63 ($C_{h'}$), 140.53 (C_9), 139.34 ($C_{3,\ g}$), 138.09 ($C_{g'}$), 132.98 ($C_{a'}$), 132.66 (C_a), 131.80 ($C_{i'}$), 130.68 (C_i), 129.41 (C_4), 128.70 (C_2), 127.58 (C_e), 127.29 ($C_{e'}$), 126.23 (C_b), 125.72 ($C_{b'}$), 123.78 ($C_{6,\ 6'}$), 123.18 (C_c), 122.45 ($C_{c'}$), 114.92 ($C_{7,\ 7'}$), 111.57 (C_d), 111.07 ($C_{d'}$), 108.15 (C_f), 107.96 ($C_{f'}$). MS (FAB): m/z 677 $[M]^+$.

Synthesis of 8a. This was prepared from dimer **3a** (70 mg, 0.068 mmol), 2-pyridine carbaldisopropylimine (24.2 mg, 0.164 mmol), and KPF_6 (25 mg, 0.136 mmol) and after work up gave **8a** as an orange solid (89 mg, 85%). Anal. Calcd for $C_{27}H_{26}F_6IrN_6P$: C, 42.02, H, 3.40, N, 10.89. Found: C, 41.92, H, 3.30, N, 10.81%. ^{1}H NMR (CD_2Cl_2): δ 9.28 (1H, s, H_5), 8.32 (1H, bd, J = 7.6, H_4), 8.24 (1H, dd, J = 2.8, 0.6, $H_{e'}$), 8.18 (1H, dd, J = 2.8, 0.6, H_e), 8.12 (1H, td, J = 7.8, 1.4, H_3), 8.02 (1H, dd, J = 5.3, 1.2, H_1), 7.48–7.45 (2H, m, $H_{2,\ g}$), 7.35 (1H, dd, J = 3.4, 0.8, $H_{d'}$), 7.34 (1H, dd, J = 3.4, 0.8, H_d), 7.11 (1H, td, J = 7.6, 1.4, H_c), 7.05 (1H, td, J = 7.6, 1.4, $H_{c'}$), 6.92–6.88 (2H, m, $H_{b,\ g'}$), 6.86 (1H, td, J = 7.3, 1.2, $H_{b'}$), 6.67–6.65 (2H, m, $H_{f,\ f'}$), 6.36 (1H, dd, J = 7.5, 1.4, $H_{a'}$), 6.22 (1H, dd, J = 7.5, 1.4, H_a), 4.11 (1H, sept, J = 6.7, H_6), 1.12 (3H, d, J = 6.5, $Me_{A\ or\ B}$), 1.01 (3H, d, J = 6.7, $Me_{A\ or\ B}$). ^{13}C NMR: 166.75 (C_5), 156.42 (C_9), 150.66 (C_1), 142.73 ($C_{h'}$), 142.51 (C_h), 139.85 (C_g), 139.64 (C_3), 138.14 ($C_{g'}$), 133.92 ($C_{a'}$), 132.63 (C_a), 131.25 (C_i), 130.56 ($C_{i'}$), 129.39 (C_4), 128.74 (C_2), 127.09 (C_e), 126.93 ($C_{e'}$), 126.85 (C_b), 126.47 ($C_{b'}$), 123.56 (C_c), 123.03 ($C_{c'}$), 111.67 ($C_{d'}$), 111.40 (C_d), 108.40, 108.34 ($C_{f,\ f'}$), 63.47 (C_6), 22.17 ($Me_{A\ or\ B}$), 21.82 ($Me_{A\ or\ B}$). MS (FAB): m/z 627 $[M]^+$.

Synthesis of 9a. This was prepared from dimer **3a** (40 mg, 0.039 mmol), glycine ethylester hydrochloride (13 mg, 0.090 mmol), pyridine–2-carboxaldehyde (10 mg, 9 μL, 0.090 mmol), triethylamine (9 mg, 12 μL, 0.090 mmol) and KPF_6 (17 mg, 0.090 mmol) and after work up gave **9a** as an orange-red solid (40 mg, 63%). Anal. Calcd for $C_{28}H_{26}F_6IrN_6O_2P$: C, 41.23, H, 3.21, N, 10.30. Found: C, 41.30, H, 3.14, N, 10.37%. ^{1}H NMR (CD_2Cl_2): δ 9.16 (1H, s, H_5), 8.26 (1H, d, J = 7.4, H_4), 8.15 (1H, d, J = 2.3, H_e), 8.11–8.07 (2H, m, $H_{3,\ e}$), 8.05 (1H, d, J = 5.5, H_1), 7.77 (1H, dd, J = 2.3, 0.8, H_g), 7.49 (1H, ddd, J = 7.4, 5.5, 1.6, H_2), 7.30 (1H, dd, J = 8.2, 0.8, H_d), 7.27 (1H, dd, J = 8.2, 1.2, $H_{d'}$), 7.06 (1H, td, J = 7.4, 1.2, H_c), 7.03 (1H, td, J = 7.8, 1.2, $H_{c'}$), 6.89 (1H, d, J = 2.3, $H_{g'}$), 6.86 (1H, td, J = 7.4, 1.2, H_b), 6.82 (1H, td, J = 7.4, 1.2, $H_{b'}$), 6.64 (1H, t, J = 2.3, $H_{f'}$), 6.61 (1H, t, J = 2.3, H_f), 6.28 (1H, dd, J = 7.4, 1.2, $H_{a'}$), 6.22 (1H, dd, J = 7.8, 1.2, H_a), 4.60 (1H, dd, J = 15.6, 1.2, H_6), 4.42 (1H, dd, J = 15.6, 1.2, H_7), 3.84 (2H, q, J = 7.0, H_8), 1.05 (3H, t, J = 7.0, Me). ^{13}C NMR: 173.57 (C_5), 167.19 (C_9), 156.12 (C_{10}), 151.50 (C_1), 143.23 ($C_{h'}$), 143.07 (C_h), 140.53 (C_g), 140.04 (C_3), 138.72 ($C_{g'}$), 134.10 ($C_{a'}$), 133.33 (C_a), 131.55 (C_i), 130.33 (C_4), 129.86 ($C_{i'}$), 129.77 (C_2), 127.33 (C_b), 127.26 ($C_{b'}$), 127.08 (C_e), 126.89 ($C_{e'}$), 124.01 (C_c), 123.88 ($C_{c'}$), 111.98 (C_d), 111.79 ($C_{d'}$), 108.79 ($C_{f'}$), 108.68 (C_f), 62.42 (C_8), 61.83 ($C_{6,\ 7}$), 14.02 (Me). MS (FAB): m/z 671 $[M]^+$.

X-ray diffraction

Data were collected on a Bruker Apex 2000 CCD diffractometer using graphite monochromated Mo-K_α radiation, λ = 0.7107 Å. The data were corrected for Lorentz and polarisation effects

Table 6 X-ray data for compounds **4a**, **5a**, **6a**, **8a** and **9a**

Compound reference	**4a**	**5a**	**6a**	**8a**	**9a**
Chemical formula	$C_{30}H_{23}BrF_6IrN_6P$ (CH_2Cl_2)	$C_{30}H_{24}F_6IrN_6P$ $(CHCl_3)$	$C_{31}H_{24}F_6IrN_6O_2P$ $(2H_2O)$	$C_{27}H_{26}F_6IrN_6P$ (CH_2Cl_2)	$C_{28}H_{26}F_6IrN_6O_2P$ $(2CH_2Cl_2)$
Formula mass	969.55	925.09	885.76	856.63	985.57
Temperature/K	150(2)	150(2)	150(2)	150(2)	150(2)
Crystal system	Monoclinic	Triclinic	Triclinic	Orthorhombic	Monoclinic
Space group	$P2(1)/c$	$P\bar{1}$	$P1$	$Pna2(1)$	$P2(1)/c$
a/Å	12.112(2)	8.6792(13)	9.6561(16)	13.521(3)	14.172(3)
b/Å	17.706(3)	13.646(2)	11.621(2)	26.046(6)	15.658(3)
c/Å	16.566(3)	14.054(2)	15.632(3)	8.728(2)	16.259(4)
α/°	90.00	89.021(3)	105.756(3)	90.00	90.00
β/°	106.849(3)	82.419(3)	99.890(3)	90.00	97.643(4)
γ/°	90.00	88.401(3)	99.000(3)	90.00	90.00
U/Å^3	3400.2(10)	1649.1(4)	1624.5(5)	3073.9(12)	3575.9(14)
No. of formula units per unit cell/Z	4	2	2	4	4
Density (calc.) $_{calc.}$/ Mg m^{-3}	1.894	1.863	1.811	1.851	1.831
Abs. coefficient/mm^{-1}	5.372	4.407	4.240	4.637	4.147
F(000)	1872	900	868	1672	1928
Crystal size mm	0.21 × 0.15 × 0.06	0.15 × 0.14 × 0.05	0.17 × 0.13 × 0.11	0.32 × 0.14 × 0.11	0.26 × 0.13 × 0.10
Theta range/°	1.72 to 25.00	1.46 to 26.00	1.86 to 26.00	1.56 to 26.00	1.45 to 26.00
Index ranges	$-14 \le h \le 14$, $-21 \le k \le 20$, $-19 \le l \le 19$	$-10 \le h \le 10$, $-16 \le k \le 16$, $-17 \le l \le 17$	$-11 \le h \le 11$, $-14 \le k \le 14$, $-19 \le l \le 19$	$-16 \le h \le 16$, $-32 \le k \le 31$, $-10 \le l \le 10$	$-17 \le h \le 17$, $-19 \le k \le 19$, $-20 \le l \le 20$
No. of reflections measured	24 390	13 007	12 736	23 204	27 403
No. of independent reflections	5999 [R_{int} = 0.0544]	6407 [R_{int} = 0.0419]	11 255 [R_{int} = 0.0277]	6016 [R_{int} = 0.0470]	7022 [R_{int} = 0.0857]
Data/restraints/ parameters	5999/0/406	6407/0/433	11 255/3/847	6016/1/399	7022/0/479
Goodness-of-fit, F^2	0.950	0.922	0.942	1.003	1.023
Final R indices $[I > 2\sigma(I)]$	0.0331, wR_2 = 0.0668	0.0387, wR_2 = 0.0689	0.0390, wR_2 = 0.0785	0.0297, wR_2 = 0.0653	0.0647, wR_2 = 0.1341
R indices (all data)	0.0433, wR_2 = 0.0691	0.0497, wR_2 = 0.0718	0.0453, wR_2 = 0.0802	0.0351, wR_2 = 0.0671	0.1099, wR_2 = 0.1489
Largest diff. peak and hole/e Å^{-3}	1.440 and −0.761	1.616 and 1.241	1.838 and −1.100	2.075 and −0.570	2.639 and −1.632

and empirical absorption corrections were applied. The structure was solved by direct methods and with structure refinement on F^2 employed SHELXTL version 6.10.[34] Hydrogen atoms were included in calculated positions (C–H = 0.93–1.00 Å, O–H = 0.84 Å) riding on the bonded atom with isotropic displacement parameters set to 1.5U_{eq} (O) for hydroxyl H atoms, 1.5U_{eq} (C) for methyl hydrogen atoms and 1.2U_{eq} (C) for all other H atoms. All non-hydrogen atoms were refined with anisotropic displacement parameters without positional restraints. Disordered solvent was removed the Squeeze option in PLATON.[35] Figures were drawn using the program ORTEP.[36] Crystal data for **4a**, **5a**, **6a**, **8a**, and **9a** are in Table 6 those for **4b** and **4c** are in the ESI, Table S1.† Coordinates have been deposited with the Cambridge crystallographic database CCDC numbers CCDC 922554–922560.

Acknowledgements

We thank the University of Leicester for funding (SS) and study leave (DLD) and Professor Mike Wolf of the University of British Columbia, Vancouver for facilities provided during the study leave, the Leverhulme Trust for a study abroad fellowship (DLD) and Johnson Matthey for a loan of $IrCl_3$. F.L thanks INSTM for funding and visiting leave from Italy to the University of British Columbia.

Notes and references

1 M. A. Baldo, S. Lamansky, P. E. Burrows, M. E. Thompson and S. R. Forrest, *Appl. Phys. Lett.*, 1999, **75**, 4–6.

2 (*a*) J. D. Slinker, A. A. Gorodetsky, M. S. Lowry, J. J. Wang, S. Parker, R. Rohl, S. Bernhard and G. G. Malliaras, *J. Am. Chem. Soc.*, 2004, **126**, 2763–2767; (*b*) M. S. Lowry, J. I. Goldsmith, J. D. Slinker, R. Rohl, R. A. Pascal, G. G. Malliaras and S. Bernhard, *Chem. Mater.*, 2005, **17**, 5712–5719; (*c*) A. B. Tamayo, S. Garon, T. Sajoto, P. I. Djurovich, I. M. Tsyba, R. Bau and M. E. Thompson, *Inorg. Chem.*, 2005, **44**, 8723–8732; (*d*) H. J. Bolink, L. Cappelli, E. Coronado, M. Gratzel and M. K. Nazeeruddin, *J. Am. Chem. Soc.*, 2006, **128**, 46–47; (*e*) M. K. Nazeeruddin, R. T. Wegh, Z. Zhou, C. Klein,

Q. Wang, F. De Angelis, S. Fantacci and M. Grätzel, *Inorg. Chem.*, 2006, **45**, 9245–9250.
3 (*a*) Y. Chi and P.-T. Chou, *Chem. Soc. Rev.*, 2010, **39**, 638–655; (*b*) C. Ulbricht, B. Beyer, C. Friebe, A. Winter and U. S. Schubert, *Adv. Mater.*, 2009, **21**, 4418–4441; (*c*) Y. You and S. Y. Park, *Dalton Trans.*, 2009, 1267–1282; (*d*) E. Baranoff, J. H. Yum, M. Graetzel and M. K. Nazeeruddin, *J. Organomet. Chem.*, 2009, **694**, 2661–2670; (*e*) W.-Y. Wong, *J. Organomet. Chem.*, 2009, **694**, 2644–2647; (*f*) E. Kim and S. B. Park, *Chem.–Asian J.*, 2009, **4**, 1646–1658.
4 (*a*) L. He, L. Duan, J. Qiao, G. Dong, L. Wang and Y. Qiu, *Chem. Mater.*, 2010, **22**, 3535–3542; (*b*) L. He, J. Qiao, L. Duan, G. Dong, D. Zhang, L. Wang and Y. Qiu, *Adv. Funct. Mater.*, 2009, **19**, 2950–2960.
5 (*a*) L. He, L. Duan, J. Qiao, R. Wang, P. Wei, L. Wang and Y. Qiu, *Adv. Funct. Mater.*, 2008, **18**, 2123–2131; (*b*) L. He, L. Duan, J. Qiao, D. Zhang, L. Wang and Y. Qiu, *Chem. Commun.*, 2011, **47**, 6467–6469.
6 G. Calogero, G. Giuffrida, S. Serroni, V. Ricevuto and S. Campagna, *Inorg. Chem.*, 1995, **34**, 541–545.
7 (*a*) P. Belser and A. V. Zelewsky, *Helv. Chim. Acta*, 1980, **63**, 1675–1702; (*b*) V. Wing-Wah Yam and V. Wing-Man Lee, *J. Chem. Soc., Dalton Trans.*, 1997, 3005–3010; (*c*) M. Maruyama and Y. Kaizu, *Inorg. Chim. Acta*, 1996, **247**, 155–159; (*d*) D. Mishra, S. Naskar, B. Adhikary, R. J. Butcher and S. K. Chattopadhyay, *Polyhedron*, 2005, **24**, 201–208; (*e*) A. C. G. Hotze, J. A. Faiz, N. Mourtzis, G. I. Pascu, P. R. A. Webber, G. J. Clarkson, K. Yannakopoulou, Z. Pikramenou and M. J. Hannon, *Dalton Trans.*, 2006, 3025–3034.
8 (*a*) Q. Zhao, L. Li, F. Li, M. Yu, Z. Liu, T. Yi and C. Huang, *Chem. Commun.*, 2008, 685–687; (*b*) K. Huang, H. Wu, M. Shi, F. Li, T. Yi and C. Huang, *Chem. Commun.*, 2009, 1243–1245; (*c*) Y. You, H. S. Huh, K. S. Kim, S. W. Lee, D. Kim and S. Y. Park, *Chem. Commun.*, 2008, 3998–4000.
9 A. J. Howarth, D. L. Davies, F. Lelj, M. O. Wolf and B. O. Patrick, *Dalton Trans.*, 2012, **41**, 10150–10152.
10 C. M. Alvarez, R. Garcia-Rodriguez and D. Miguel, *Dalton Trans.*, 2007, 3546–3554.
11 (*a*) M. S. Lowry, W. R. Hudson, R. A. Pascal and S. Bernhard, *J. Am. Chem. Soc.*, 2004, **126**, 14129–14135; (*b*) J. I. Goldsmith, W. R. Hudson, M. S. Lowry, T. H. Anderson and S. Bernhard, *J. Am. Chem. Soc.*, 2005, **127**, 7502–7510.
12 P. J. Spellane, R. J. Watts and C. J. Curtis, *Inorg. Chem.*, 1983, **22**, 4060–4062.
13 (*a*) M. V. Narayana Reddy, G. C. Sekhar Reddy, K. S. Kumar, C. S. Reddy and C. N. Raju, *J. Heterocycl. Chem.*, 2010, **47**, 538–542; (*b*) I. Zaltsgendler, Y. Leblanc and M. A. Bernstein, *Tetrahedron Lett.*, 1993, **34**, 2441–2444.
14 D. L. Davies, M. P. Lowe, K. S. Ryder, K. Singh and S. Singh, *Dalton Trans.*, 2011, **40**, 1028–1030.
15 In complex **4b**, so not in table, see cif.
16 M. Ghedini, A. Golemme, I. Aiello, N. Godbert, R. Termine, A. Crispini, M. La Deda, F. Lelj, M. Amati and S. Belviso, *J. Mater. Chem.*, 2011, **21**, 13434–13444.
17 The spectrum for **6a** was decomposed as well but since the substituent on the aryl had little effect on the predicted bands it was felt that **4a** and **5a** were sufficiently good models for the TDDFT studies.
18 The parameters used for decomposition are listed in the ESI (Table S3 and Fig. S6†).
19 J. Tomasi, B. Mennucci and R. Cammi, *Chem. Rev.*, 2005, **105**, 2999–3094.
20 T. B. de Queiroz, M. B. S. Botelho, J. M. Fernández-Hernández, H. Eckert, R. Q. Albuquerque and A. S. S. de Camargo, *J. Phys. Chem. C*, 2013, **117**, 2966–2975.
21 Experimental spectra were adjusted to remove any negative absorbance.
22 J. S. Sears, T. Koerzdoerfer, C. R. Zhang and J. L. Bredas, *J. Chem. Phys.*, 2011, 135.
23 Similar distortions in geometry have been seen in salicylimine complexes see for example ref. 16 and S. Liu, H. Sun, Y. Ma, S. Ye, X. Liu, X. Zhou, X. Mou, L. Wang, Q. Zhao and W. Huang, *J. Mater. Chem.*, 2012, **22**, 22167–22173.
24 Y. Zhao and D. G. Truhlar, *Theor. Chem. Acc.*, 2008, **120**, 215–241.
25 M. J. Frisch, G. W. Trucks, H. B. Schlegel, G. E. Scuseria, M. A. Robb, J. R. Cheeseman, G. Scalmani, V. Barone, B. Mennucci, G. A. Petersson, H. Nakatsuji, M. Caricato, X. Li, H. P. Hratchian, A. F. Izmaylov, J. Bloino, G. Zheng, J. L. Sonnenberg, M. Hada, M. Ehara, K. Toyota, R. Fukuda, J. Hasegawa, M. Ishida, T. Nakajima, Y. Honda, O. Kitao, H. Nakai, T. Vreven, J. A. Montgomery, Jr., J. E. Peralta, F. Ogliaro, M. Bearpark, J. J. Heyd, E. Brothers, K. N. Kudin, V. N. Staroverov, R. Kobayashi, J. Normand, K. Raghavachari, A. Rendell, J. C. Burant, S. S. Iyengar, J. Tomasi, M. Cossi, N. Rega, N. J. Millam, M. Klene, J. E. Knox, J. B. Cross, V. Bakken, C. Adamo, J. Jaramillo, R. Gomperts, R. E. Stratmann, O. Yazyev, A. J. Austin, R. Cammi, C. Pomelli, J. W. Ochterski, R. L. Martin, K. Morokuma, V. G. Zakrzewski, G. A. Voth, P. Salvador, J. J. Dannenberg, S. Dapprich, A. D. Daniels, Ö. Farkas, J. B. Foresman, J. V. Ortiz, J. Cioslowski and D. J. Fox, Gaussian, Inc., Wallingford, CT, 2009.
26 D. Escudero and L. González, *J. Chem. Theor. Comput.*, 2012, **8**, 203–213.
27 C. Adamo and V. Barone, *J. Chem. Phys.*, 1999, **110**, 6158–6170.
28 T. H. Dunning Jr. and P. J. Hay, in *Modern Theoretical Chemistry*, ed. H. F. Schaefer III, Plenum, New York, 1976, vol. 3, pp. 1–28.
29 A. Nicklass, M. Dolg, H. Stoll and H. Preuss, *J. Chem. Phys.*, 1995, **102**, 8942–8952.
30 G. Scalmani and M. J. Frisch, *J. Chem. Phys.*, 2010, **132**, 114110.
31 S. Portman, Molekel4.3 CSCS/ETHZ, 2002.

32 C. F. Macrae, I. J. Bruno, J. A. Chisholm, P. R. Edgington, P. McCabe, E. Pidcock, L. Rodriguez-Monge, R. Taylor, J. v. d. Streek and P. A. Wood, *J. Appl. Crystallogr.*, 2008, **41**, 466–470.
33 R. Bauernschmitt and R. Ahlrichs, *J. Chem. Phys.*, 1996, **104**, 9047–9052.
34 *Bruker, Version 6.10*, Bruker Inc., Madison, Wisconsin, USA, 1998–2000.
35 P. Vandersluis and A. L. Spek, *Acta Crystallogr., Sect. A: Fundam. Crystallogr.*, 1990, **46**, 194–201.
36 L. J. Farrugia, *J. Appl. Crystallogr.*, 1997, **30**, 565.